Kinetic Properties of Alfvén Modes in Tokamak Plasmas

Ph. Lauber, S. Günter, M. Brüdgam*, A. Könies†, S.D. Pinches** and ASDEX-Upgrade Team*

*Max-Planck-Institut für Plasmaphysik, EURATOM-Association, D-85748 Garching, Germany
†Max-Planck Institut für Plasmaphysik, EURATOM-Association, D-17489 Greifswald, Germany
**UKAEA Fusion Association Culham Science Centre, Abingdon, Oxfordshire OX143DB UK

Abstract. The ability to predict the stability of fast-particle-driven Alfvén eigenmodes in burning fusion plasmas requires a detailed understanding of the dissipative mechanisms that damp these modes. In order to address this question, the linear gyro-kinetic, electromagnetic code LIGKA[1] is employed to investigate their behaviour in realistic tokamak geometry. The eigenvalue formulation of LIGKA allows to calculate self-consistently the coupling of large-scaled MHD modes to the gyroradius scale-length kinetic Alfvén waves. Therefore, the properties of the kineticly modified TAE mode in or near the gap (KTAE, radiative damping or 'tunnelling') and its coupling to the continuum close to the edge can be analysed numerically. In addition, an antenna-like version of LIGKA allows for a frequency scan, analogous to an external antenna.
The model and the implementation of LIGKA were recently extended in order to capture the coupling of the shear Alfvén waves to the sound waves. This coupling becomes important for the investigation of kinetic effects on the low-frequency phase of cascade modes [2], where e.g. geodesic acoustic effects play a significant role [3, 4].

Keywords: Kinetic Alfvén Waves, TAE, KTAE, Cascade Modes
PACS: 52.65.Tt, 52.55.Pi

INTRODUCTION

The stability properties of the toroidal Alfvén Eigenmode (TAE) [5],[6] in magnetically confined fusion plasmas are of great interest because TAEs can be driven unstable by fusion-born α-particles with dangerous consequences for the overall plasma stability and confinement [7]. In order to make predictions for an ignited plasma like ITER, the background damping mechanisms of TAEs have to be investigated carefully. These mechanisms are electron and ion Landau damping, continuum damping, collisional damping and radiative damping. The latter mechanism requires a non-perturbative description, since the MHD properties of the mode structure are modified by coupling to the kinetic Alfvén wave (KAW) [8].

The application of perturbative, fluid models like CASTOR-K [9] and NOVA-K [10] on JET for low-n, low-m cases resulted in damping rates which were too small by one order of magnitude compared to the measured damping rates [11] [12]. With a gyrokinetic, perturbative extension of CASTOR-K based on a complex resistivity model [13] considerably higher damping rates with a discrepancy of a factor of 2 were calculated, verifying the importance of mode conversion of Alfvén and kinetic Alfvén eigenmodes. The global gyrokinetic wave code PENN [14] found agreement with the experiment,

CP871, *Theory of Fusion Plasmas: Joint Varenna-Lausanne International Workshop,*
edited by J. W. Connor, O. Sauter, and E. Sindoni

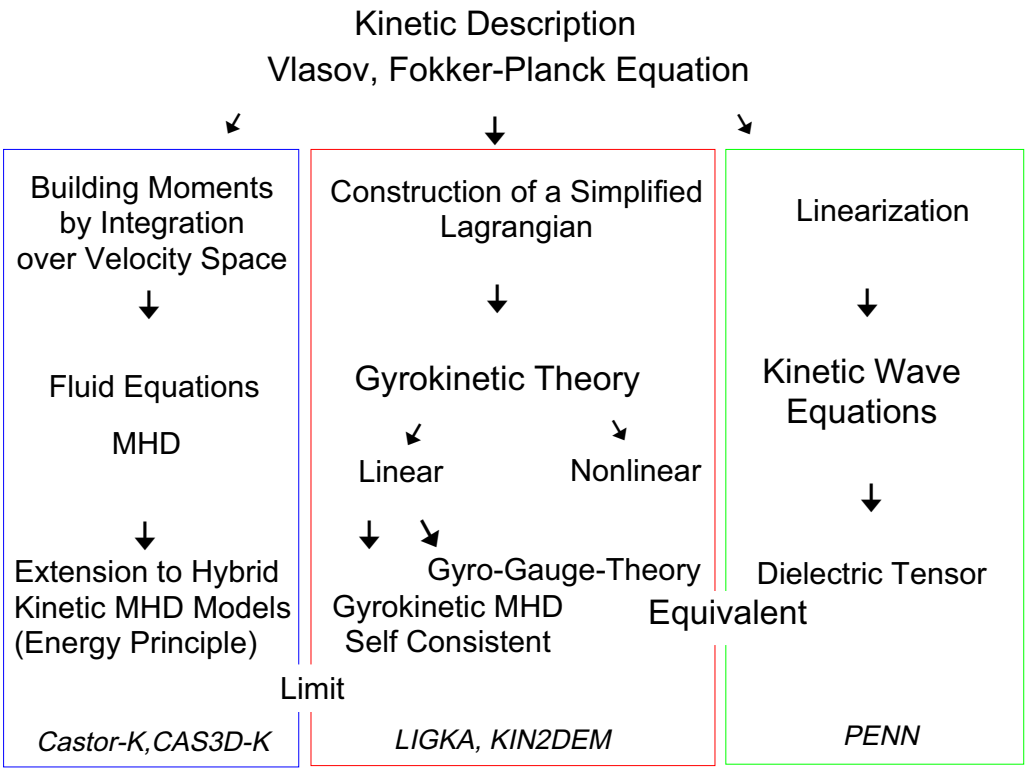

FIGURE 1. Overview: kinetic models

proposing mode conversion in the plasma centre as the main damping mechanism. However, there has been no confirmation of this mechanism by analytical estimates or other codes like CASTOR-K. Recent work on this topic, employing a global, reduced kinetic model [15] did not confirm any significant mode conversion mechanism in the centre. Instead, continuum damping near the plasma edge was found to be important, leading to damping rates comparable to the experiment.

The application of the gyrokinetic, linear, non-perturbative code LIGKA[1] to this problem resulted [16] in similar results as the 'reduced kinetic model' [15]. Benchmarks with this reduced model and the axisymmetric version of CAS3D-K [17, 18, 19] showed good agreement for electron damping, continuum damping and radiative damping. Strong mode conversion in the plasma centre like in PENN was also not found.

LIGKA is based on a self-consistent model by Qin et al. [20][21] consisting of the quasi-neutrality equation and the moment equation for the perturbed current. It is non-perturbative, since it allows for a non-linear dependence of the eigenvalue through the velocity space integrals and also for a mode structure which is not prescribed by ideal MHD calculations. The propagator integrals along the drift orbit of ions and electrons are carried out numerically using the drift kinetic code HAGIS [22],[23], and the resonance integrals are solved accurately applying rational interpolation and grid refinement techniques. LIGKA therefore covers all the damping mechanisms mentioned above, except collisional damping, which is assumed to be small compared to the other types of damping.

LIGKA was originally developed and tested for the Alfvén-frequency regime. It is shown in this paper how the model can be extended and modified for lower frequencies, i.e. the drift and the sound waves. First test cases are shown.
This extension starts to become important when e.g. the low-frequency phase of Alfvén cascade modes is investigated [3]. An analysis with the MHD-code CASTOR [24] shows that cascade modes can exist above the magneto-acoustic continuum branches at low-frequencies and that they do not transform directly into TAE modes when the q-profile drops. There are strong indications that these modes were observed in the early phase of several ICRH-heated ASDEX-Upgrade discharges.

THEORETICAL MODEL AND RELEVANT LIMITS

As shown in [16], the contact between the reduced kinetic model and the linear gyrokinetic model can be obtained as summarised below:
The following basic equation [27] is usually employed as the relevant one for non-ideal shear Alfvén modes:

$$\nabla_\perp \cdot \frac{\omega^2}{v_A^2}\nabla_\perp \phi + \frac{\partial}{\partial s}\nabla_\perp^2 \frac{\partial \phi}{\partial s} = \delta_s^2 \frac{\omega}{c}\nabla_\perp^4 \frac{\partial A_\parallel}{\partial s} - \frac{3}{4}\frac{\omega^2}{v_A^2}\rho_i^2 \nabla_\perp^4 \frac{\partial A_\parallel}{\partial s} \tag{1}$$

It is derived from the vorticity equation with finite Larmor radius (FLR) corrections and Ohm's law given in references [25], [26]. Here, ϕ is the electrostatic potential, $A_\parallel \mathbf{b}$ the magnetic vector potential, r the radial coordinate and s the coordinate along the field line. δ_s is the skin depth $\delta_s = c^2\varepsilon_0/\omega\sigma$ with σ being the parallel complex electrical conductivity, which was chosen to be $\sigma/\varepsilon_0 = i\omega_{pe}^2/(\omega + i\nu_{eff} - k_\parallel^2 v_{the}^2/\omega)$. ω_{pe} and ν_{eff} are the electron plasma frequency and the effective electron collision frequency.
Near the singular layer of the ideal MHD equation (left hand side of equation 1), the right hand side becomes most important and can be simplified by the substitutions $i\omega A_\parallel/c \to \partial\phi/\partial s$, $\partial/\partial s \to ik_\parallel \equiv i\Big(n - m/q(r)\Big)/R$, $\omega^2/\omega_A^2 \equiv \Omega^2 = \Omega_m^2 \equiv 1/4q_m^2$ to yield a coupled system of fourth-order differential equations with the right hand side reducing to

$$-r_{LT}^2 \Omega_m^2 \frac{\partial^4 \phi_m}{\partial r^4}. \tag{2}$$

with

$$r_{LT}^2 = \frac{3}{4}\rho_i^2 + \rho_s^2 = \rho_i^2 \left\{ \frac{3}{4} + \frac{T_e}{T_i}\left[1 + \frac{v_A^2}{v_{the}^2}(1 + \frac{\nu_{eff}}{|k_\parallel| v_A})\right]\right\}. \tag{3}$$

The underlying equations of LIGKA (derived by Qin [20],[21]) consist of the quasi-neutrality equation

$$0 = \sum_a \Big[\int d^2\mathbf{v} J_0 f_a + \frac{e_a}{m_a}\nabla_\perp \frac{n_{a0}}{B^2}\nabla_\perp \phi(\mathbf{x}) + \frac{3e_a v_{th,a}^2 n_{a0}}{4m_a\Omega_a^4}\nabla_\perp^4 \phi(\mathbf{x})\Big] \tag{4}$$

and the gyrokinetic moment equation:

$$
\begin{aligned}
- \quad & \frac{\partial}{\partial t}\frac{e}{m}\nabla_\perp \frac{n_0}{B^2}\nabla_\perp \phi + \nabla A_\parallel \times \mathbf{b}\cdot\nabla(\frac{\nabla\times\mathbf{B}}{B}) + (\mathbf{B}\cdot\nabla)\frac{(\nabla\times\nabla\times\mathbf{A})\cdot\mathbf{B}}{B^2} \\
= \quad & -\sum_a e_a \int \mathbf{v}_d\cdot\nabla J_0 f_a d^3\mathbf{v} + \frac{c}{v_{A0}^2}\frac{3v_{th,a}^2}{4\Omega_a^2}\nabla_\perp^4\frac{\partial\phi(\mathbf{x})}{\partial t} + \\
& \mathbf{B}\cdot\nabla\Big(\frac{4\pi e_a^2 n_{a0} v_{th,a}^2}{2Bm_a c^2\Omega_a^2}\nabla_\perp^2 A_\parallel\Big) + \mathbf{b}\times\nabla(\frac{2\pi e_a n_{0a} v_{th,a}^2}{B\Omega_a})\cdot\nabla\nabla^2\phi \qquad (5)
\end{aligned}
$$

Here, $\sum_a$ indicates the sum over different particle species with the perturbed distribution function f_a, mass m_a, charge e_a, unperturbed density n_{a0}, thermal velocity $v_{th,a} = \sqrt{T_a/m_a}$ and cyclotron frequency Ω_a. The perturbed distribution function f_a is governed by the linearised Vlasov equation:

$$
\frac{\partial f}{\partial t} + (v_\parallel \mathbf{b} + \mathbf{v}_d)\cdot\nabla f = (\frac{e\mathbf{b}}{eB}\times\nabla F_0)\cdot\nabla H_1 + \frac{\partial F_0}{\partial\varepsilon}(v_\parallel\mathbf{b}+\mathbf{v}_d)\cdot\nabla H_1
$$

with

$$
H_1 = eJ_0(\phi - v_\parallel(\nabla\psi)_\parallel/i\omega).
$$

Now one can split up a term that gives a 0-th order solution of the GKE and that allows to write most terms proportional to $(\phi-\psi)$, i.e. the electrostatic contribution:

$$
f = g + H_1\frac{\partial F_0}{\partial\varepsilon}; \quad g = h - \left[e\frac{\partial F_0}{\partial\varepsilon} - \frac{c}{i\omega B}\nabla F_0\cdot(\mathbf{b}\times\nabla)\right]J_0\psi_\parallel
$$

Integrating this expression over the velocity space gives the convective pressure term:

$$
\int e\frac{\mathbf{v}_d}{\omega}\cdot\nabla f d^3\mathbf{v} \approx \int e\frac{\mathbf{v}_d}{\omega}\cdot\nabla h d^3\mathbf{v} + \frac{c\mathbf{b}}{\omega}\times(\frac{\nabla B}{B} + \mathbf{b}\cdot\nabla\mathbf{b})\cdot\nabla(\frac{c\nabla p}{i\omega B}\cdot\mathbf{b}\times\nabla)\psi_\parallel
$$

In the same simple limit as described above, carrying out the velocity space integrals and using $A_\parallel = c(\nabla\psi)_\parallel/i\omega$, these equations can be reduced to:

$$
[1+\xi_e Z(\xi_e)](\phi-\psi) = T_e/T_i\rho_i^2\nabla_\perp^2\phi \qquad (6)
$$

and

$$
\nabla_\perp\cdot\frac{\omega^2}{v_A^2}\nabla_\perp\phi + \frac{\partial}{\partial s}\nabla_\perp^2\frac{\partial\psi}{\partial s} = \frac{3}{4}\rho_i^2\frac{\omega^2}{v_A^2}\nabla_\perp^4\phi \qquad (7)
$$

leading by elimination of ψ to exactly the same fourth order equation as given above in lines 1 and 2.

The sound-wave dispersion relation can be obtained by applying the cold ion, hot electron expansion to the QN equation:

$$
\rho_s^2 k_\perp^2\phi = (\frac{c_s^2 k_\parallel^2}{\omega^2} - 1 + \frac{\omega_{*e}}{\omega})(\phi-\psi); \qquad \frac{\omega^2}{v_A^2}\phi - k_\parallel^2\psi = 0
$$

It can be easily seen that the sound wave is basically electrostatic and it's coupling to the shear Alfvén wave depends on $\beta = 2c_s^2/v_A^2$.
For the complete spectrum of waves, including the fast compressional wave, one would need the full set of three equations rather than the two equations considered here [28, 29]. In addition to ϕ and ψ one would need an equation for the perturbed parallel magnetic field compression $\delta B_{\|}$. However, for the frequency regime considered here, the only effect of this third equation is to eliminate the ∇B-drifts in favour of the curvature drifts [28].
The next limit considered here is the geodesic-acoustic correction to the Alfvén continuum. It is well known that this correction influences the low-frequency behaviour of the cascade modes [3]. This correction is

$$\frac{\omega^2}{v_A^2} - k_{\|}^2 - \frac{2c_s^2}{v_A^2 R_0^2}(1 + \frac{1}{2q_0^2}) = 0; \quad c_s^2 = \gamma p_0/n_0 \tag{8}$$

This expression can be derived from the linear ideal MHD-equations. The term $\frac{1}{2q_0^2}$ is due to the toroidal coupling of the Alfvén waves to the acoustic wave. If a kinetic closure is employed, c_s has to be replaced by $\hat{c}_s^2 = (T_e + (7/4)T_i)/m_i$ [30]. Also kinetic expressions for the toroidal acoustic coupling and the $k_{\|}$-corrections have been derived [31, 32].
In order to recover this correction from the equations underlying LIGKA, one has to keep $\omega_d = \omega_k + \omega_B$ as an operator of first order in the radial direction. The expression for h reads as follows:

$$h = \frac{ie}{T} F_0 \sum_m \int_{-\infty}^{t} dt' e^{i[n(\varphi'-\varphi) - m(\theta'-\theta) - \omega(t'-t)]} e^{-im\theta} \cdot (\omega - \omega_*^T) J_0 \cdot \tag{9}$$
$$[\phi_m(r') - (1 - \frac{\omega_d(\theta')}{\omega})\psi_m(r')]$$

Carrying out the integration in the simplest limit and employing the ω_B-cancellation described above, one obtains for the quasi-neutrality equation:

$$2\tau \frac{\langle \omega_k \rangle}{\omega}\phi + \rho_s^2 k_{\perp}^2 \phi = (\frac{c_s^2 k_{\|}^2}{\omega^2} - 1 + \frac{\omega_{*e}}{\omega})(\phi - \psi) \tag{10}$$

with

$$\langle \omega_k \rangle = \frac{v_{thi}^2}{\omega_{ci}} \mathbf{b} \times (\mathbf{b} \cdot \nabla \mathbf{b}) \cdot \nabla$$

The same procedure is employed for the GKM equation:

$$\nabla_{\perp} \cdot \frac{\omega^2}{v_A^2} \nabla_{\perp} \phi - k_{\|} \nabla_{\perp}^2 k_{\|} \phi = i\mu_0 \omega^2 \sum_a \int d^3 v (e \frac{\omega_d}{\omega} J_0 h)_a$$

One can see clearly, that there are two extra contributions to the second order operator in radial direction: one term is coming from the electrons,

$$\frac{4\tau^2 \langle \omega_k \rangle^2}{\omega^2}\phi,$$

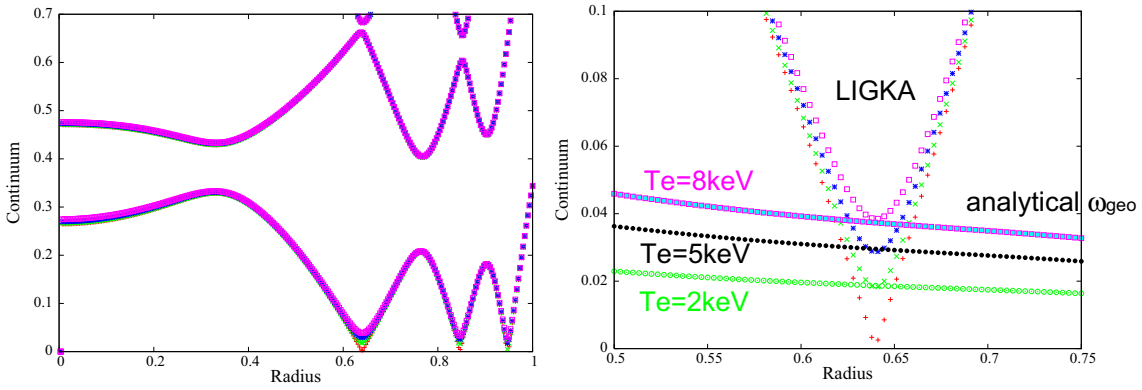

FIGURE 2. Alfvén Continuum for different electron temperatures (left), detail (right). Comparison of the analytical ω_{geo} (lines) with the local LIGKA results

the other from the ions:

$$\frac{7\langle\omega_k^2\rangle}{\omega^2}\phi.$$

Note the difference between $\langle\omega_k^2\rangle$ and $\langle\omega_k\rangle^2$. Expanding these two operators gives exactly the continuum correction as given in line 8 with c_s^2 replaced by $\hat{c}_s^2$.
In LIGKA, the integrals over the unperturbed orbits and over velocity space are carried out numerically. In order to check the correctness of these integrations, the terms for the second order operator were collected and a local solve carried out: figure 2 shows, that for $n = 1$, $m = 2$ and $q(r_s) = 2$ with $r_s = 0.64$, $k_{||}$ goes to zero for zero temperature. For increasing temperature ($T_e = T_i$) the correction due to the acoustic coupling can be easily identified and compared with the analytical values as given by line 8. Good agreement is found in this first, simple benchmark.

Numerical Model

The basic version of LIGKA [1] solves the equations 4,5 and the linear gyrokinetic equation for the perturbed distribution function f up to 2. order in $k_\perp \rho_i$. As discretisation scheme finite elements based on Hermite polynomials in radial direction (with usually 200 to 400 grid-points along the minor radius) and a Fourier decomposition in the poloidal angle are employed. There is no coupling in the toroidal angle. Using a Galerkin method an eigenvalue problem is formed. The boundary conditions are chosen as $\phi_m(0) = \phi_m(a) = \psi_m(0) = \psi_m(a) = 0$. Straight field line coordinates for the background quantities given by the equilibrium code HELENA [24] are chosen. Since the velocity space integrals depend on the eigenfrequency ω in a complicated way (resonance integrals), the eigenvalue problem is not linear anymore, and LIGKA applies the Nyquist contour integration technique to find the eigenvalues.
To be able to study the complex physics that is caused by non-ideal effects in and near the gap region, LIGKA has been modified:
For examining the rich spectrum around a gap, many closely spaced modes are expected.

Using a Nyquist solver is cumbersome under these conditions because many poles require a high number of sample points along the integration contour, even when also background phase removal techniques are applied [33]. Thus an antenna-like version of LIGKA was developed: a drive vector is added on the right hand side of the homogeneous equation:

$$M(\omega)\begin{pmatrix}\phi\\ \psi\end{pmatrix} = \mathbf{d} \tag{11}$$

where $\mathbf{d}$ is only nonzero for the last finite element at the plasma edge, prescribing a small perturbation from the outside. The absolute value of $\mathbf{d}$ is chosen somewhat arbitrarily. However, it was tested that different choices of $\mathbf{d}$ did not change the basic properties of the response spectrum,i.e. the location and the width of the peaks. The wave equations in the vacuum and the proper boundary conditions are not considered in this simple model. The eigenfunctions are found by inverting $M(\omega)$ resulting in:

$$\mathbf{I}\begin{pmatrix}\phi\\ \psi\end{pmatrix} = M(\omega)^{-1}\mathbf{d}, \tag{12}$$

and the plasma response is 'measured' by an integral over the eigenfunction:

$$\mathscr{R} = \sum_m \int_0^a \phi_m \phi_m^* dr \tag{13}$$

Recently, for this antenna version, a parallelised solver has been implemented: using the Watson Sparse Matrix Package by IBM [34], with compressed matrix storage and distributed memory, the performance of LIGKA has been improved considerably. Thus problems with higher n and more poloidal modes can be addressed.

LOW-FREQUENCY CASCADE MODES

In a series of discharges at ASDEX-Upgrade (#20396-99) chirping events in the early phase of the discharge were observed [35]. As can be seen in figure 3, in these shots on-axis ICRH is applied at 0.9 seconds and is ramped up to 4MW. In this figure also the magnetic spectrogram of a Mirnov-coil measurement is shown: the coil B31-14 is located on the outboard midplane, measuring mainly radial perturbations. From a phase correlation analysis of different coils one can clearly identify, that the set of modes at around 260 kHz are TAE-modes with the toroidal mode numbers $n = 4,5,6,7$. However, the chirping events starting at 1.05 seconds and 1.09 also have most likely a mode number of $n = 5$. Therefore, these modes cannot be conventional cascade modes that would convert into TAE-modes when the minimum value of the q-profile, q_{min} reaches $q_{TAE} = 2m - 1/2n$. Furthermore, the onset-frequency of these chirping modes is below $f_{geodesic}$ which is the lower bound for a conventional Alfvén cascade.

It is known from reflectometry measurements that the chirping modes are very core localised [35], $r_{mode} < 0.3$. Taking into account the onset of the sawtooth modes at 1.32 seconds and a sawtooth inversion radius of $r \approx 0.3$ one can obtain a rough estimate of the q-profile based on an ASTRA-simulation with a fast particle pressure given by

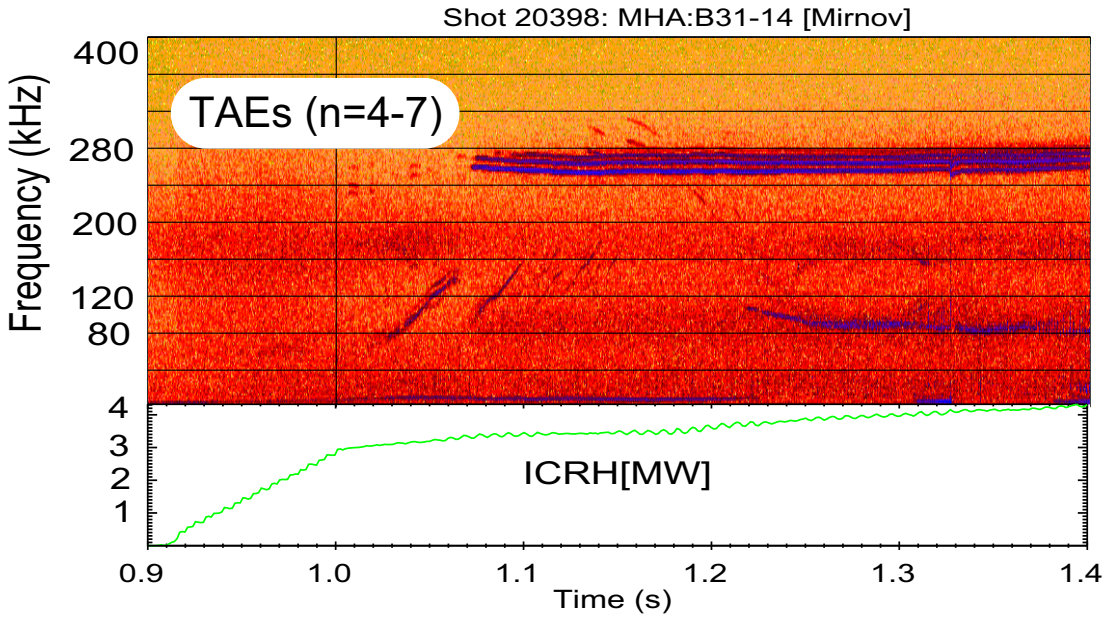

FIGURE 3. Time evolution of the magnetic spectrogram (top) and the IRCH power (bottom) for ASDEX-Upgrade shot #20398

a TORIC-calculation. The evolution of the $q-$profile is shown in figure 4. Based on these $q-$profiles a series of equilibria were constructed and the Alfvén continua were calculated with the linear MHD-code CASTOR [24]. The inclusion of compressibility strongly changes the spectrum compared to a pure Alfvénic case in this relatively low-frequency region. One can see that there is a local maximum in the continuum at $r = 0.1$ (see figure 4) starting from $\omega/\omega_A = 0.15$ and going up to $\omega/\omega_A = 0.23$ which fits reasonably to the experimental chirping range.

Using CASTOR, one finds a cascade-like mode just slightly above this maximum, as shown in figure 5, bottom row. This mode exhibits a typical cascade-like perturbation in the radial direction, i.e. a mainly cylindrical behaviour, however, in the direction parallel to the equilibrium magnetic field one finds a strong $v_{||}$-perturbation, whose amplitude is comparable in magnitude to the radial perturbation. This perturbation is dominated by a strong sideband coupling to the neighbouring $m+1$ and $m-1$ harmonics.
This first analysis will be refined with future experiments, taking advantage of a more complete set of diagnostics, such as the Soft-X-ray cameras and the fast-particle-loss detector.

CONCLUSIONS

In this paper it has been shown that the gyrokinetic formulation underlying LIGKA recovers the reduced kinetic model, the sound wave dispersion relation and the geodesic-acoustic corrections and is therefore not only applicable to the physics of kinetically modified global shear Alfvén modes but also to the lower-frequency modes in the sound-wave regime. First test cases were shown.

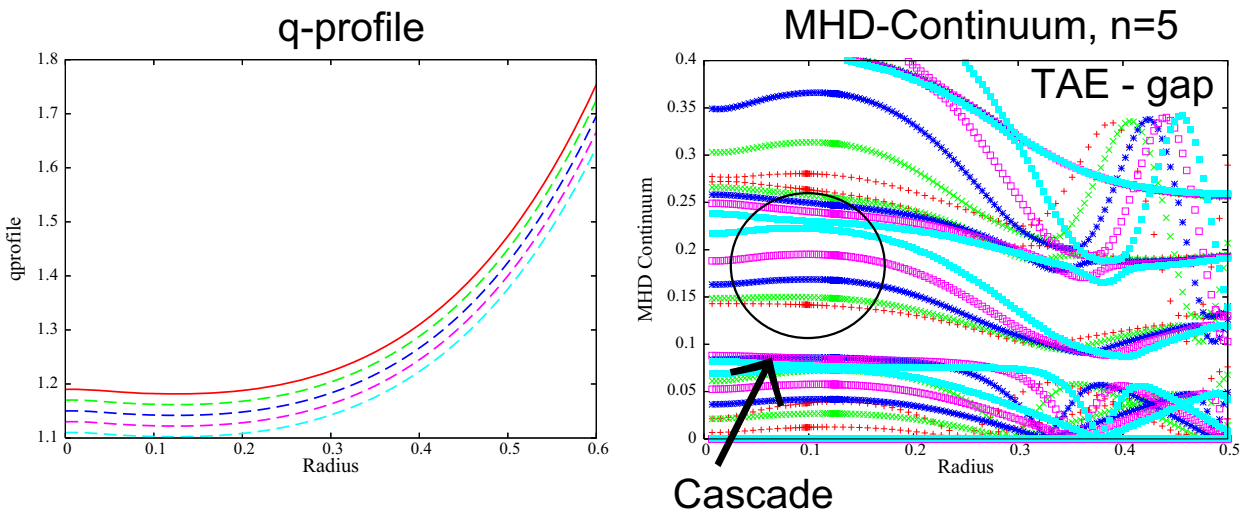

FIGURE 4. q-profile evolution (left) and Alfvén continuum for 5 different time points. As the q-profile drops, the maximum of the Alfvén continuum branch (within the circle) rises (right, units normalised to ω_A). This causes the cascade mode sitting on top of this branch to chirp up in frequency. Here, ω_A is $3.1 \cdot 10^6$ rad/s resulting in a chirp from about 70 to 120 kHz. Including a correction due to toroidal rotation gives reasonable agreement with the experimental values of 80 to 140 kHz.

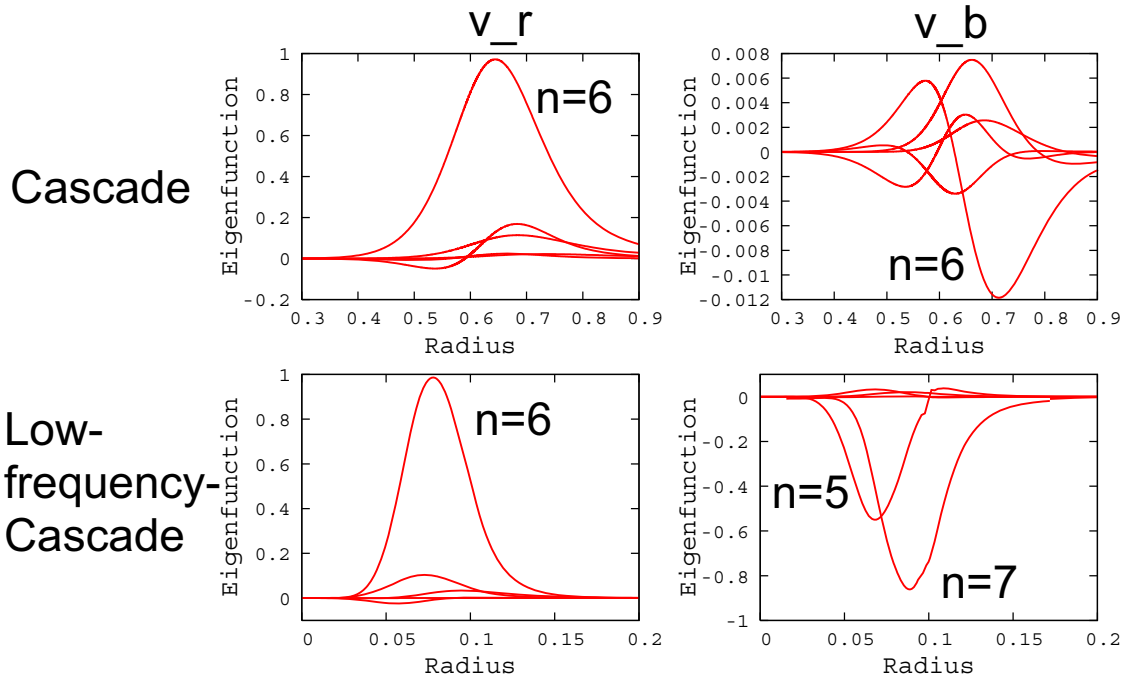

FIGURE 5. CASTOR-eigenfunctions for the radial (left) and parallel (right) velocity perturbation of a conventional Alfvén cascade (top) and a low-frequency cascade (bottom)

Chirping events in the early phase of ASDEX-Upgrade discharges might be explained by low-frequency cascade modes that show a strong sideband coupling to neighbouring poloidal harmonics.

ACKNOWLEDGMENTS

The authors thank G. Fu (PPPL, Princeton) and H.L. Berk (IFS, Austin) for numerous discussions and invaluable input for this work. The TORIC-calculations were carried out by R. Bilato, the ASTRA simulations by G. Pereverzev.

REFERENCES

1. Lauber, Ph.,'Linear Gyrokinetic Description of Fast Particle Effects on the MHD Stability in Tokamaks', Ph.D. Thesis, TU München, (2003)
2. S.E. Sharapov et al., Phys. Plasmas **9**, 2027 (2002)
3. B.N. Breizman, M.S. Pekker and S.E. Sharapov et al., Phys. Plasmas **12**, 112506 (2005)
4. G.Y. Fu and H. L. Berk, Phys. Plasmas **13**, 052502 (2006)
5. C.Z. Cheng, L. Chen, M.S. Chance, Annals of Physics **161**, 21 (1985)
6. C.Z. Cheng, M.S. Chance, Phys. Fluids **29**, 11 (1986)
7. G.Y. Fu, J.W. VanDam, Phys. Fluids **1**, 1949 (1989)
8. R.R. Mett, S.M. Mahajan, Phys. Fluids B **4**, 2885 (1992)
9. D. Borba, W. Kerner, J. Comput. Phys **153**, 101 (1999)
10. G.Y. Fu,C.Z. Cheng, R. Budney et al., Phys. Plasmas **3**, 4036 (1996)
11. A. Fasoli, A. Jaun, D. Testa, Phys. Lett. A **265**, 288 (2000)
12. D. Testa, Y. Fu, A. Jaun et al., Nucl. Fusion **43**, 594 (2003)
13. D. Borba et al., Nucl. Fusion **42**, 1029 (2002)
14. A. Jaun et al., CPC **92**, 153 (1995)
15. G.Y. Fu,H. L. Berk, A. Pletzer, Phys. Plasmas **13**, 052502 (2006)
16. Ph. Lauber, S. Günter, S.D. Pinches, Phys. Plasmas **12**, 122501 (2005)
17. A. Koenies, IAEA TCM Meeting, Goeteborg (2001)
18. C. Nuehrenberg, Phys. Plasmas **6**, 137 (1998)
19. C. Nuehrenberg, Plasma Phys. Control. Fusion **41**, 1055 (1999)
20. H. Qin, 'Gyrokinetic Theory and Computational Methods for Electromagnetic Perturbations in Tokamaks', Ph.D. Thesis, Princeton University (1998)
21. H. Qin,W.M. Tang, G.Rewoldt, Phys. Plasmas **5**, 1035 (1998)
22. S. D. Pinches, Ph.D. Thesis, The University of Nottingham, (1996)
23. S. D. Pinches et al., CPC **111**, 131 (1998)
24. G.T.A. Huysmans. J.P. Goedbloed, W. Kerner, Proc. CP90 Conf. on Comp Phys.Proc., Wolrd Scientific Publ.Co., p. 371 (1991)
25. A. Hasegawa, L. Chen, Phys. Rev. Lett. **35**, 370 (1975)
26. A. Hasegawa, L. Chen, Phys. Fluids **19**, 1924 (1976)
27. H.L Berk, R.R. Mett, and D.M. Lindberg, Phys. Fluids B **5**, 3969 (1993)
28. W.M. Tang, J.W. Connor, R.J. Hastie, Nucl. Fusion **20**, 1439 (1980)
29. F. Zonca, L. Chen and R. Santoro, Plasma Phys. Controlled Fusion **38**, 2011 (1996)
30. V. A. Mazur, and A.B. Mikhailovskii, Nucl. Fusion **17**,193 (1977)
31. H. Sugama and T.-H. Watanabe, Phys. Plasmas **13**, 012501 (2006)
32. H.L. Berk, private communication
33. S. Brunner, private communication
34. A. Gupta, IBM Research Report, RC 21888 (2000)
35. S. Graca, private communication